

1

ABSTRACT

1 RNTUPLE FOR ATLAS ANALYSIS WORKFLOWS

2 Fatima Rodriguez, M.A.
3 Department of Physics
4 Northern Illinois University, 2025
5 Hector de la Torre, Director

6 RNTuple is the new data storage format set to replace TTree at the start of the High
7 Luminosity LHC. An investigation was conducted on how analysis workflows for ATLAS re-
8 searchers will change with RNTuple. Additionally, performance studies have been conducted
9 that demonstrate an improvement in speed and memory usage at the analysis front. Finally,
10 different compression algorithms were tested and it was found that blah blah remains to best
11 work with RNTuple.

NORTHERN ILLINOIS UNIVERSITY
DE KALB, ILLINOIS

DECEMBER 2025

RNTUPLE FOR ATLAS ANALYSIS WORKFLOWS

BY

FATIMA RODRIGUEZ
© 2025 Fatima Rodriguez

A DISSERTATION SUBMITTED TO THE GRADUATE SCHOOL
IN PARTIAL FULFILLMENT OF THE REQUIREMENTS
FOR THE DEGREE
MASTER OF PHYSICS

DEPARTMENT OF PHYSICS

Dissertation Director:
Hector de la Torre

13

ACKNOWLEDGEMENTS

14

Thanks thanks

DEDICATION

15

Thanks thanks

TABLE OF CONTENTS

	Page
¹⁷ LIST OF FIGURES	^{vi}
Chapter	
¹⁸ 1 INTRODUCTION	¹
¹⁹ 1.1 Phenomenology at the LHC	²
²⁰ 1.2 Physics Quantities	⁵
²¹ 1.2.1 Invariant Mass	⁵
²² 2 THE ATLAS EXPERIMENT	⁷
²³ 2.1 The Large Hadron Collider	⁷
²⁴ 2.2 The ATLAS Apparatus	⁹
²⁵ 2.2.1 The Inner Detector	¹⁰
²⁶ 2.2.2 Calorimeter Systems	¹¹
²⁷ 2.2.3 Muon Spectrometer	¹²
²⁸ 2.2.4 Magnet System	¹³
²⁹ 2.2.5 ATLAS Trigger System	¹⁴
³⁰ 2.3 HL-LHC and HL-ATLAS	¹⁴
³¹ 3 ATLAS SOFTWARE AND COMPUTING	¹⁶
³² 3.1 ROOT Introduction	¹⁶
³³ 3.1.1 TTree Introduction	¹⁷
³⁴ 4 RNTUPLE	²⁰
³⁵ 4.1 Data Structure	²⁰

	Page
37 Chapter	Page
36 4.2 UI	21
38 4.2.1 C++	22
39 4.2.2 RDataFrame	22
40 5 RNTUPLE VS. TTREE	23
41 5.1 Readability Speed	23
42 5.2 Writing Speed	24
43 5.2.1 Output Sizes	25
44 5.3 Memory Consumption	27
45 5.4 Compression Algorithms Study	27
46 6 ANALYSIS GRAND CHALLENGE: RNTUPLE IMPLEMENTATION	28
47 6.1 RDataFrame Analysis Workflow	28
48 6.1.1 Event Selections	28
49 6.2 TTree vs. RNTuple AGC	29
50 6.2.1 Timing Measurements	32
51 6.2.1.1 LZ4 vs. ZSTD Input Files	33
52 REFERENCES	34
53 APPENDIX: OBJECTIVE SYMPTOMS	39

LIST OF FIGURES

	Figure	Page
55	1.1 The SM..	4
56	1.2 Summary of SM cross-section Measurements	5
57	2.1 CERN Complex	8
58	2.2 ATLAS Schematics	10
59	2.3 ATLAS ID Schematics.	11
60	2.4 ATLAS Calorimeter System.	12
61	2.5 ATLAS Muon Spectrometer.	13
62	3.1 DataChain	17
63	3.2 TTree Data Structure	19
64	4.1 RNTupleStructure.	21
65	5.1 Loading Histogram Times	24
66	5.2 Output Histogram Times.	26
67	5.3 Memory Measurements	27
68	6.1 ttbar	29
69	6.2 top mass	30
70	6.3 Ht	31
71	6.4 Ht	32

72	6.5 LZ4	33
----	-------------------	----

CHAPTER 1

INTRODUCTION

75 Our current understanding of the building blocks of our universe is summarized with
76 one model, called the Standard Model (SM) [4]. From the way we power our cities, to the
77 particles that hold them together, the SM explains how the basic building blocks of matter
78 interact, governed by fundamental forces: electromagnetism, the strong force and the weak
79 force. Yet, questions remain about the SM, such as is there a unification theory that includes
80 gravity? Why are there only three generations of fundamental particles? What is the nature
81 of dark matter and dark energy, and how does it fit within the SM? What about the origin of
82 the matter-antimatter asymmetry? Is the SM complete or do other exotic particles exists?
83 Over the years, experimental particle physicists and engineers have built technology to test
84 the SM, either by performing precision measurements of particles and their behaviors, or by
85 colliding particles and measuring their outputs. As a result, we have increased our confidence
86 in the SM theory, but continue to search for answers for these remaining questions through
87 experimental discovery.

88 A Toroidal LHC Apparatus (ATLAS) [2] is a particle physics experiment designed to
89 detect the high-energy particle collisions from the Large Hadron Collider (LHC) [29]. At the
90 LHC, collisions take place at a rate of more than a billion interactions per second, which
91 is a combined data volume of about 60 million megabytes per second [34]. In order to
92 extend its discovery potential, the LHC will have a major upgrade to increase the number
93 of instantaneous collision rate. This upgrade, called the High-Luminosity LHC (HL-LHC)
94 [35], will require a new data storage format that can handle this increase in data.

95 RNTuple [32] is the new ROOT [27] data storage format that will be in use at the start of
96 the HL-LHC [24]. RNTuple takes advantage of modern C++ techniques, which have shown
97 to improve read speedability and memory usage when compared to its predecessor, TTree,
98 and other data storage formats such as HDF5 and Parquet [28]. RNTuple is currently under
99 heavy development. Its base format has only recently left the experimental stage and many
100 tools and capabilities built around it are still evolving.

101 This thesis investigates the performance of RNTuple for ATLAS analysis workflows. This
102 chapter will provide a more detailed introduction of the SM, followed by an introduction
103 to the ATLAS experiment and its detector technology in Chapter 2. In Chapter 3, the
104 ATLAS software and computing system, and data contents are introduced. In Chapter 4,
105 an introduction to RNTuple and TTree is provided along with examples of how RNTuple
106 is applied in comparison to TTree. Performance studies conducted for RNTuple and how
107 they compare with TTree will be presented in Chapter 5. In Chapter 6, the Analysis Grand
108 Challenge (AGC) is introduced along with its RNTuple implementation. A final discussion
109 and conclusions are given in Chapter 7.

110 1.1 Phenomenology at the LHC

111 The SM is a quantum field theory that explains and catagorizes all observed funda-
112 mental particles by their properties and interactions. Quantum field theory (QFT) is the
113 main theoretical tool for describing particle interactions by combining special relativity and
114 quantum mechanics. Due to this combination, QFT is a probabilistic theory where each
115 particle has an associated field that permeates all of space; therefore, forces are simply the
116 interactions between these different fields. For example, the electromagnetic force is just
117 the interaction between the electromagnetic field and charged matter fields, which fall under

¹¹⁸ quantum electrodynamics (QED). In sum, the SM encompasses all known elementary parti-
¹¹⁹ cle interactions, except for gravity, through a collection of quantum field theories: QED, the
¹²⁰ Glashow-Weinberg-Salam theory of electroweak processes, and quantum chromodynamics.

¹²¹ The four groups of particles shown in Figure 1.1: quarks, leptons, gauge bosons, and
¹²² scalar bosons, can be further categorized as *bosons* or *fermions* because of a fundamental
¹²³ property called spin. Similar to the Earth, particles carry orbital angular momentum and
¹²⁴ spin angular momentum; however, for particles, spin is an intrinsic property. All bosons carry
¹²⁵ an integer spin; while, fermions carry half-integer spin. As a result from QFT, each fermion
¹²⁶ has an antiparticle with the same mass and lifetime as the particle itself, but are oppositely
¹²⁷ charged. The three charged leptons (e , μ , τ) are massive, while their corresponding neutrinos
¹²⁸ (ν_e , ν_μ , ν_τ), are massless with neutral charge. Due to QCD, there are 8 types of gluons. The
¹²⁹ Higgs boson has its own section as a scalar boson because unlike the vector bosons with
¹³⁰ spin 1, the Higgs boson has spin 0. In sum, there are a total of 12 leptons including their
¹³¹ antiparticles, 36 quarks including all the flavors and their antiparticles, 12 vector bosons,
¹³² and 1 scalar boson, which makes a total of 61 fundamental particles.

¹³³ Collider experiments serve as probes to the SM because they directly test conservation
¹³⁴ laws through the detection of final state radiation. In colliders, two beams of particles are
¹³⁵ accelerated to reach high energies and brought together for collision. Each collision is called
¹³⁶ an event and specific interactions or transformations are called processes. Processes are
¹³⁷ governed by conservation laws, such as conservation of energy and charge. For example,
¹³⁸ due to the conservation of energy, the energy in the center of mass frame must be greater
¹³⁹ than the sum of masses of the produced particles. When high-energy charged particles
¹⁴⁰ pass through matter, they ionize atoms along their path, which then serve as "seeds" for
¹⁴¹ cloud chambers or sparks for sparks chambers. Their classification is then calculated by the
¹⁴² energy differences detected from those "seeds". For neutral particles, their reconstruction
¹⁴³ is calculated using the conservation of momentum. Through QFT, the rate of a process,

Standard Model of Elementary Particles

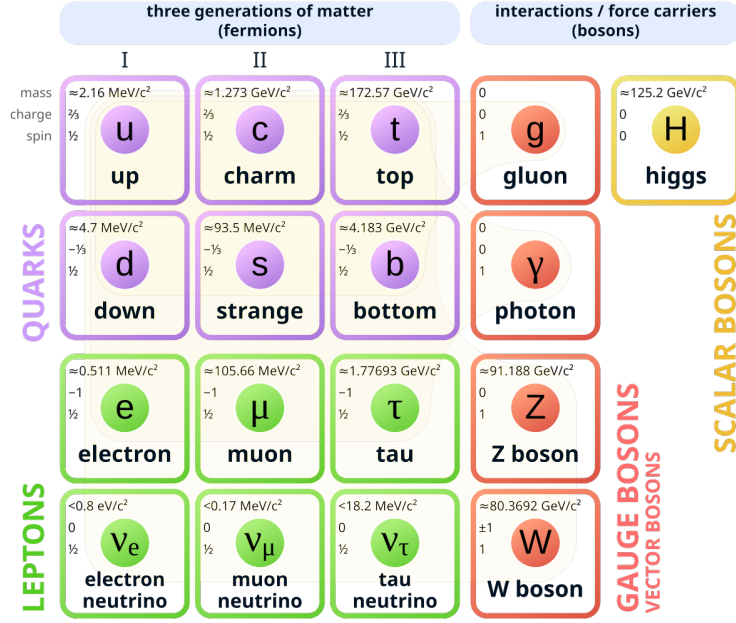


Figure 1.1: Particle content of the Standard Model [?].

¹⁴⁴ called cross-sections, can be predicted via the particle kinematics, their properties, and the
¹⁴⁵ properties of the process. Experimentally, cross-sections can be calculated via Equation 1.1,
¹⁴⁶ where N is the number of events for the process being measured and L is the instantaneous
¹⁴⁷ luminosity, defined in Equation as 1.2.

$$\sigma = \frac{N}{\int L dt} \quad (1.1)$$

¹⁴⁸

$$L = f \frac{n_1 n_2}{4\pi \sigma_x \sigma_y} \quad (1.2)$$

¹⁴⁹ f is the frequency of collisions, n_1 and n_2 are the number of particles in the colliding bunches.
¹⁵⁰ σ_x and σ_y are the root-mean-squared horizontal and vertical beam sizes. Figure 1.2 displays
¹⁵¹ the predicted cross-sections for certain processes and the required center of mass energies for
¹⁵² those processes to be observed.

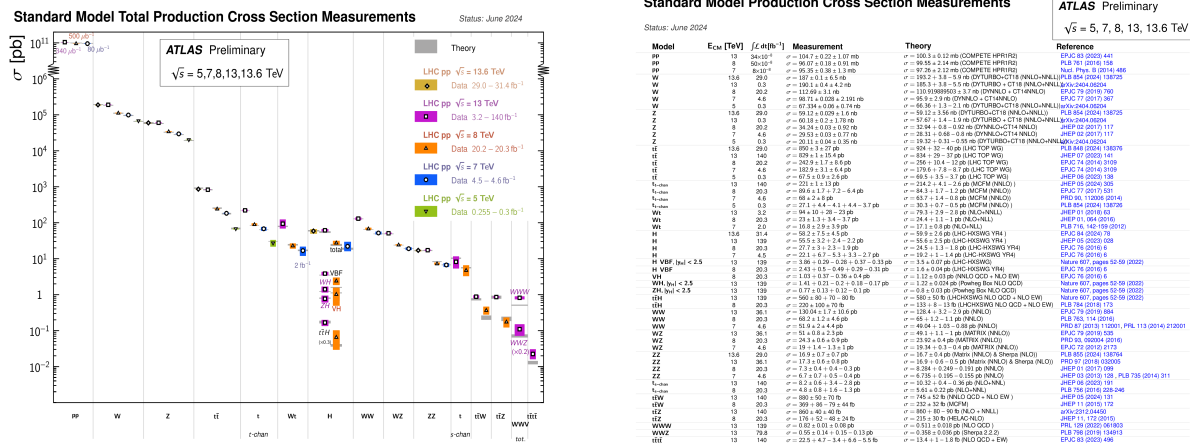


Figure 1.2: Summary of several Standard Model cross-section measurements (a) with associated references (b) [1]. Processes with smaller cross-sections are considered rare-processes because it has a lower probability of being observed. Increasing the probability of these rare-processes would require an increase of energy. The measurements are corrected for branching fractions, compared to the corresponding theoretical expectations.

153

1.2 Physics Quantities

154

This section will cover some relevant physics quantities.

155

1.2.1 Invariant Mass

Invariant mass is a quantity that characterizes a system's total energy and momentum independent of the overall motion of the system [36]. Due to special relativity, space and time coordinates are linked but dependent on a frame of reference. Lorentz transformations are used to convert coordinates from reference frame to another, and 4-vectors are used to simplify these transformations [37]. A 4-vector is a vector in spacetime with 4 quantities, such as the position 4-vector with quantities x,y,z, and time. There is also the 4-momentum vector with energy and momentum in x, y, and z directions as quantities. These 4-vectors are convenient because invariant quantities can be calculated by taking the sum of their quanti-

₁₆₄ ties squared. Invariant mass is calculated using Equation ??, where p_x, p_y, p_z is momentum
₁₆₅ in the x, y, z directions and E is energy.

$$m = \sqrt{\sum E^2 - \sum p_x^2 - \sum p_y^2 - \sum p_z^2} \quad (1.3)$$

CHAPTER 2

THE ATLAS EXPERIMENT

168 ATLAS was designed to be a general-purpose experiment, optimized to search for the
169 Higgs boson, top quark decays, and supersymmetry. In July 1997, the ATLAS Experiment
170 was approved and by November 2008, ATLAS was the largest detector ever constructed at
171 44 meters long and 25 meters in diameter. By November 2009, ATLAS recorded its first
172 proton-proton collision and by December 2010, ATLAS was first to observed the production
173 of top quark pairs, which are the heaviest known elementary particle with a strong coupling
174 to the Higgs boson. By July 2012, both ATLAS and the Compact Muon Spectrometer
175 (CMS) experiment successfully observed the Higgs boson [12, 13]. ATLAS is projected to
176 continue operation until 2035 to continue searching for standing questions from the SM.
177 This chapter will serve as an introduction to the LHC, the ATLAS detector, and upgrades
178 occurring for the HL-LHC.

2.1 The Large Hadron Collider

180 The LHC is a two-ring-superconducting-hadron accelerator and collider built outside of
181 Geneva, Switzerland at the Conseil Europeen pour la Recherche Nucleaire (CERN) [29].
182 It was approved for construction in 1996 to search for beyond the SM physics at energies
183 larger than 10 TeV. Its approval was heavily influenced by the cost-saving idea of reusing
184 the existing 26.5 km tunnels from the Large Electron-Positron (LEP) collider [14]. The LHC
185 has four main collision points that house the ATLAS, CMS, Large Hadron Collider beauty
186 (LHCb) [46], and A Large Ion Collider Experiment (ALICE) [47]. ATLAS and CMS are

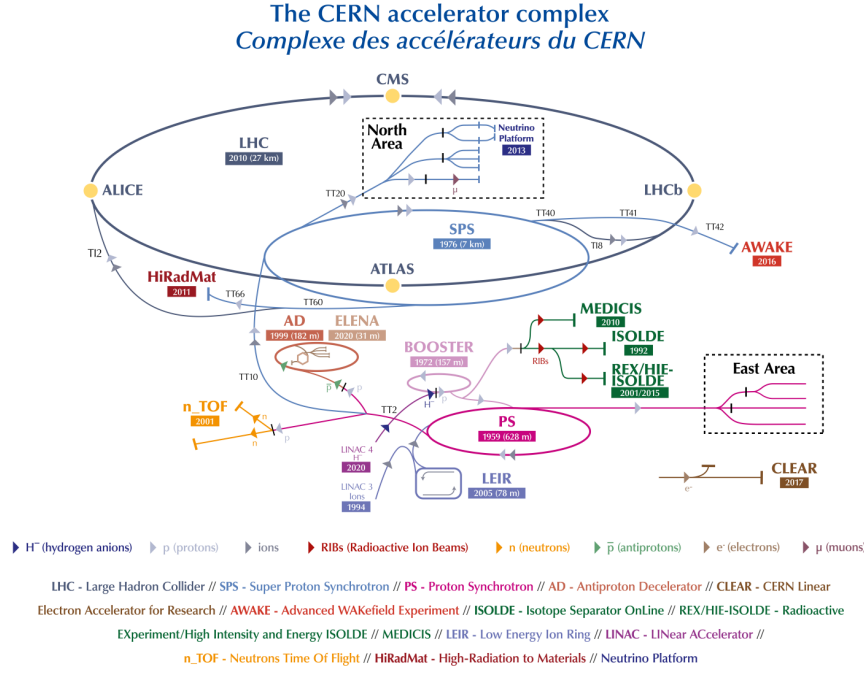


Figure 2.1: The CERN accelerator complex [15].

187 the two high-energy experiments located at diametrically opposite straight sections. LHCb
 188 is a low luminosity experiment dedicated to investigate the difference between matter and
 189 anti-matter by detecting b quarks. ALICE is an ion experiment dedicated to studying quark-
 190 gluon plasma forms.

191 The LHC is initially supplied with protons from the injector complex, which is a sequence
 192 of accelerators shown in Figure 2.1. The three main components within each of these accel-
 193 erators are magnets, vacuum chambers, and radiofrequency (RF) cavities. Superconducting
 194 magnets are responsible for guiding the beams, and vacuum chambers ensure that particles
 195 do not interact with external residual gas molecules. RF cavities are metallic chambers
 196 located inside the beam vacuum. They are designed to resonate at specific frequencies to
 197 provide small energy boosts when particles pass through.

198 As of Run 3, the LHC has collided protons at a center of mass energy of $\sqrt{s} = 13.6$ TeV
 199 and a peak instantaneous luminosity of $L = 2.1 \times 10^{34} \text{ cm}^{-2} \text{ s}^{-1}$, which have surpassed original
 200 design. Beams are delivered in bunches with bunch separation of 25 ns, corresponding to a
 201 bunch crossing frequency of 40 MHz.

202 **2.2 The ATLAS Apparatus**

203 The ATLAS detector, shown in Figure 2.2, consists of a collection of subsystems confined
 204 in a 46m long, 25m in diameter cylinder, 100m below ground. The first subsystem is the
 205 Inner Detector (ID), which is responsible for tracking charged-particles. A calorimeter system
 206 follows and measures the energy loss of the particles passing through the detector. The final
 207 subsystem is the Muon Spectrometer (MS), which measures the deflection of muons within
 208 a magnetic field using a trigger and high precision tracking chambers. Additionally, a first-
 209 level and high-level trigger system is implemented to select interesting events and record
 210 them to disk.

211 ATLAS uses a cylindrical coordinate system (r, η, ϕ) for detector design, reconstruction
 212 and data analysis. The polar coordinates, (r, ϕ) , point in the plane towards the center of the
 213 LHC ring and upwards. The pseudorapidity, η , is defined in Equation 2.1, where θ is the
 214 polar angle and equal to the true rapidity defined in Equation 2.2.

$$\eta = -\ln(\tan \frac{\theta}{2}) \quad (2.1)$$

215

$$y = \frac{1}{2} \ln \left(\frac{E + p_z}{E - p_z} \right) \quad (2.2)$$

216 The ID tracks particles in the range $|\eta| < 2.5$, the calorimeter system covers $|\eta| < 4.9$, and
 217 the MS detects muon in the $|\eta| < 2.7$ range.

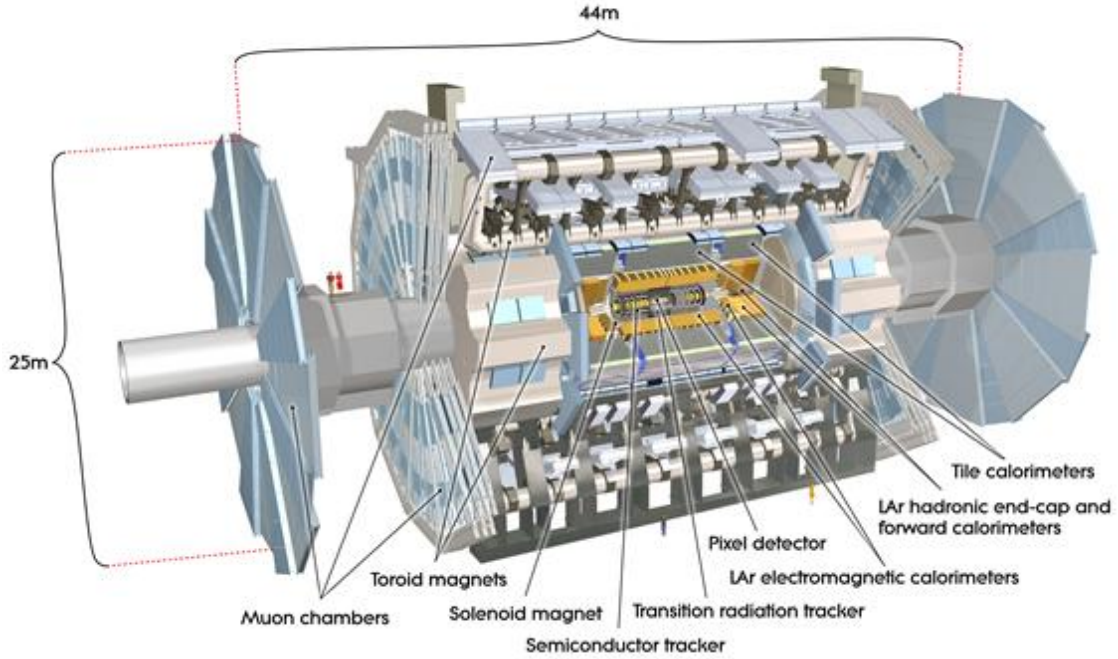


Figure 2.2: Computer generated image of the whole ATLAS detector [16].

218

2.2.1 The Inner Detector

219 The main components of the ID are the Pixel Detector, Semiconductor Tracker (SCT),
 220 and the Transition Radiation Tracker (TRT). This layout is provided in Figure 2.3. The
 221 Pixel Detector is first to pick up the energy deposits of the collisions at a precision of $10\mu m$.
 222 Their signals determine the origin and momentum of the particles. The SCT surrounds
 223 the Pixel Detector, which measures particle tracks with a precision of up to $25 \mu m$. The
 224 TRT is the final layer that provides particle type information, in combination with the other
 225 information gained in the ID.

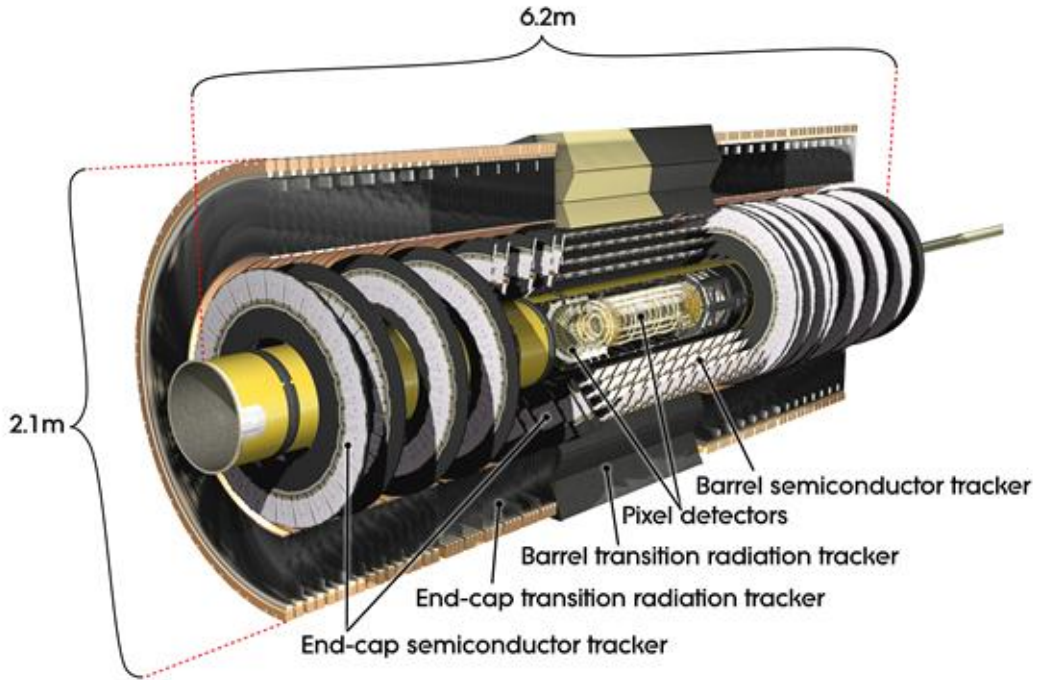


Figure 2.3: Computer generated image of the ATLAS inner detector [17].

226

2.2.2 Calorimeter Systems

227 Calorimeters are detectors that measure the energies and positions of charged and neutral
228 electromagnetically or strongly interacting particles. They consists of highly-dense materials
229 that force particles to deposit their energy. That energy is then converted into a measur-
230 able signal using layers of "active" media. The calorimeter systems consists of two types
231 of calorimeters as shown in Figure 2.4: electromagnetic and hadronic. Electromagnetic
232 calorimeters are used to measure charged particles like electrons, positrons, and photons.
233 Hadronic calorimeters are designed to detect hadrons, such as quarks, protons, and neu-
234 trons.

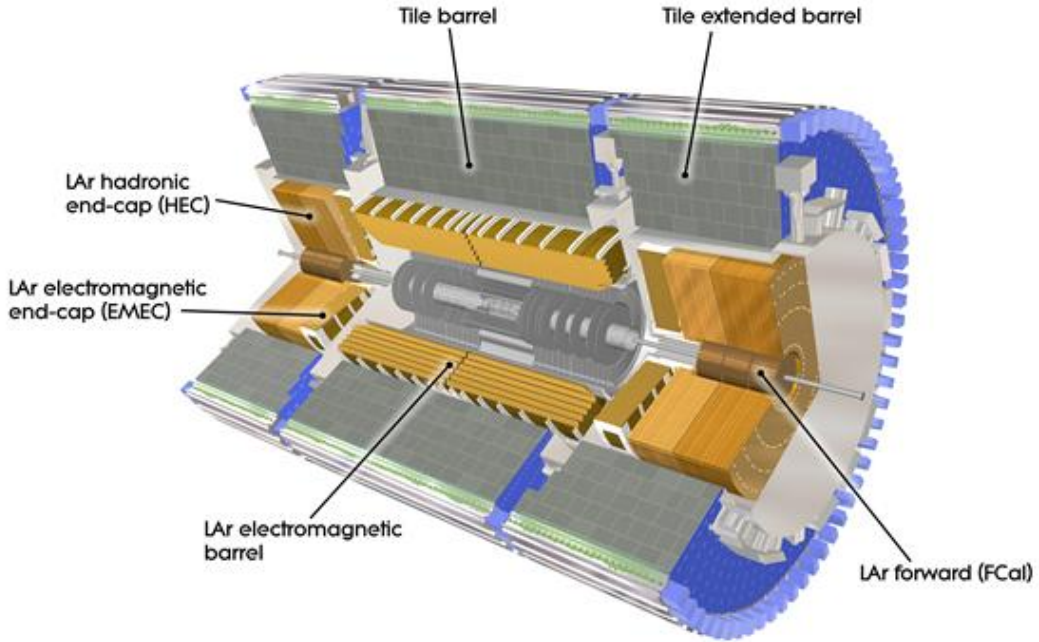


Figure 2.4: Computer generated image of the ATLAS Liquid Argon [18].

235

2.2.3 Muon Spectrometer

236 The muon spectrometer, shown in Figure 2.5, is the outer part of the ATLAS detector,
 237 designed to measuring the momentum of muons. Muons are minimally ionizing particles,
 238 meaning they can travel to the edge and beyond the ATLAS detector. The magnetic field
 239 that bends their directerries is generated by superconducting air-core toroidal magnets. There
 240 are also three stations of precision chambers consisting of layers of Monitored Drift Tubes
 241 (MDTs). The MDTs allow muons to knock out electrons from gas when passing through,
 242 to produce a signal. The New Small Wheels (NSW) sit in these endcap regions to detect
 243 charged-particle background that get produced as luminosity increases. Two chambers sit
 244 surrounding the central region and ends of the experiment: the Resistive Plate Chambers

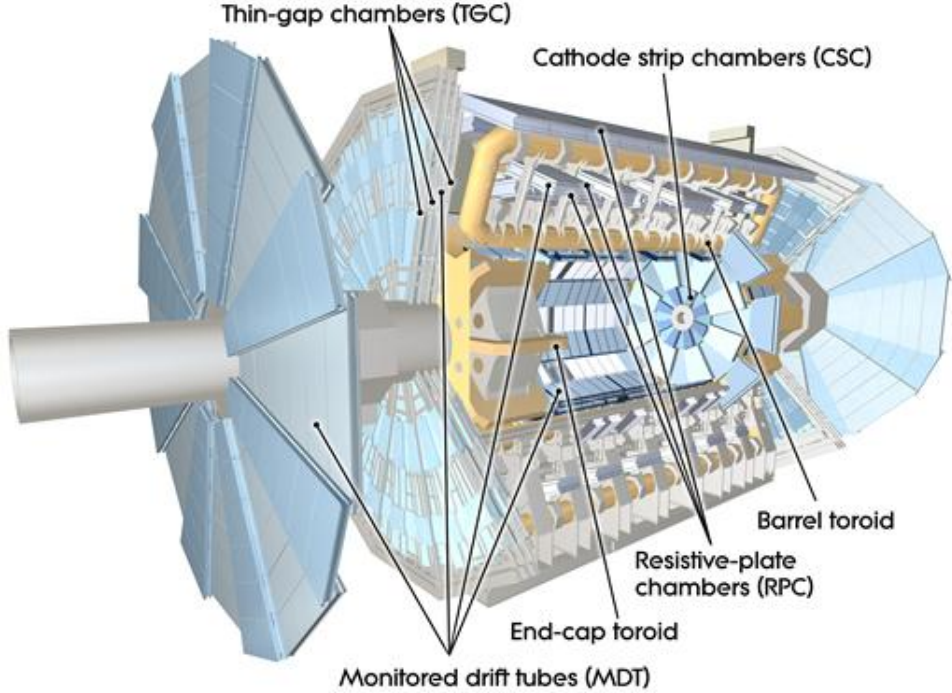


Figure 2.5: Computer generated image of the ATLAS Muons subsystems [19].

²⁴⁵ (RPCs) and Thin Gap Chambers (TGCs). They both detect muons when they ionise the
²⁴⁶ gas mixtures to generate signal.

²⁴⁷

2.2.4 Magnet System

²⁴⁸ The two main magnet systems are the Central Solenoid Magnet and the Toroid Magnets.
²⁴⁹ Generally, superconducting magnets are required to bend the directories of charged particles,
²⁵⁰ allowing for the ATLAS detector to measure their momentum and charge. The Central
²⁵¹ Solenoid Magnet provides a 2 Tesla magnetic field surrounding the inner detector. The
²⁵² Toroid Magnets are located at the ends of the experiment, and a massive toroid magnet
²⁵³ surrounds the center of the experiment. As mentioned in the previous section, the magnets
²⁵⁴ at the ends of the experiment are to bend muons for the Muon spectrometer.

255

2.2.5 ATLAS Trigger System

256 The ATLAS Trigger system is a collection of electronics that make rapid decisions of
 257 saving certain events into disk. There are two trigger subsystems that help selectively read
 258 out and store data from interesting physics events. The first level of the trigger system,
 259 called the L1 trigger, uses reduced-granularity information from the calorimeters and muon
 260 system to search for signatures of these events. The maximum L1 accept rate is 100 kHz,
 261 meaning all processing for an event must be completed within that time window. The second
 262 level of the trigger system, called L2 trigger, performs a more thorough reconstruction in
 263 just 200 μ s of the events passed in L1 to then finally pass to a data storage system for offline
 264 analysis.

265

2.3 HL-LHC and HL-ATLAS

266 The HL-LHC was proposed in 2010 to extend the discovery potential of the LHC by
 267 increasing its instantaneous luminosity (rate of collisions) by a factor of five beyond the
 268 original design value and the integrated luminosity (total number of collisions) by a factor
 269 ten. Increasing the total number of collisions will increase the probability for ATLAS and
 270 CMS to observe rare processes at higher precision, as highlighted in reference [38]. The
 271 HL-LHC configuration relies on innovations in accelerator technology such as cutting edge
 272 11 to 12 Tesla superconducting magnets, novel magnet designs, compact superconducting
 273 RF cavities for beam rotation with phase control, new technologies and materials for beam
 274 collimation, and high-current superconducting links with almost zero energy dissipation.

275

The ATLAS experiment will also require an upgrade following the HL-LHC. New sub-
 276 detectors will be installed such as the Inner Tracker [39], the High Granularity Timing

²⁷⁷ Detector [40], and additional Muon chambers [41]. There will also be different electronics
²⁷⁸ upgrades such as the Liquid Argon Calorimeter [42], the Tile Calorimeter [43], the Muon
²⁷⁹ Spectrometer [44], and the Trigger and Data Acquisition (TDAQ) system [45].

280

CHAPTER 3

281

ATLAS SOFTWARE AND COMPUTING

282 The data collected from the ATLAS data acquisition system must be compared to a set of
283 simulated data. This dataset aims to mimic the different physics processes: it's production by
284 the colliding beams, the evolution of the collision products within the detector and materials,
285 and the detector's response to ultimately interpret efficiencies and background processes.
286 Except for collision data, the output of all these data processing steps are stored in ROOT
287 files. It starts off with Monte Carlo (MC) simulations, which is a computational technique
288 that uses random sampling to generate events. Given these events, the interactions within
289 the detector and the detector's response is simulated. This reconstructed product is called an
290 Analysis Object Data (AOD), which are then cleaned by compressing the data and cutting
291 any unnecessary events or columns into a finalized product called Derived AOD (DAOD). A
292 ROOT file is produced at each step and are validated using different software tools. These
293 tools collectively encompass the software framework called Athena [31]. The flow of this
294 process is display in Figure 3.1. This chapter will provide an introduction to ROOT, its
295 data storage format TTree and RNTuple.

296

3.1 ROOT Introduction

297 ROOT is a unified software package developed for processing, analyzing, visualizing and
298 ultimately storing the massive high-energy physics datasets into a compressed binary file,
299 called a root file. Previously, high-energy experiments used FORTRAN-based libraries;
300 however, an upgrade was needed to handle the scales and complexities of the data from the

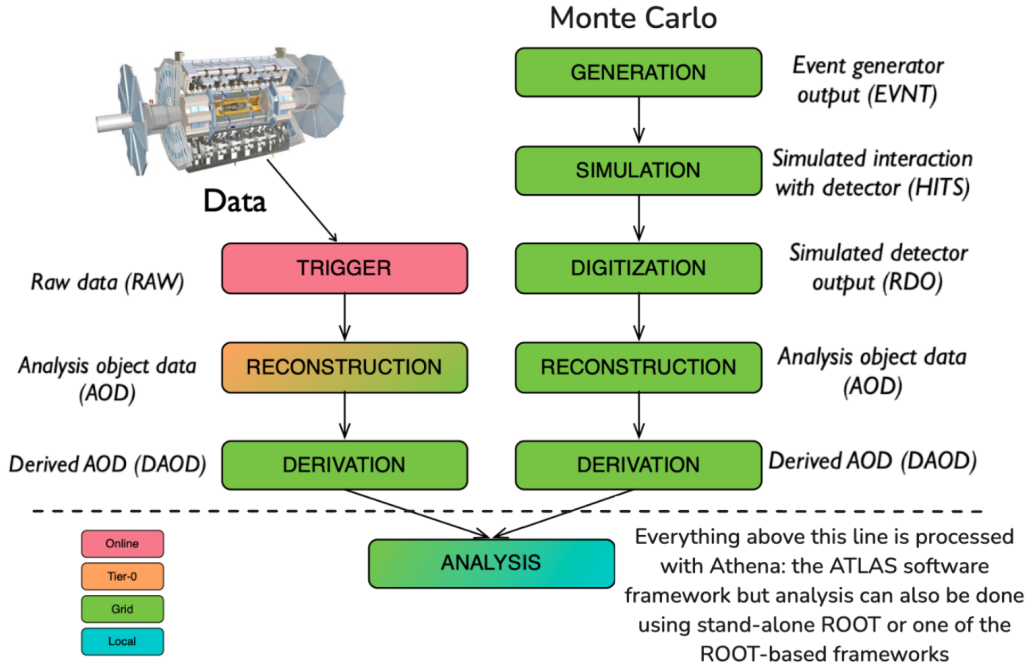


Figure 3.1: ATLAS data chain-processing for data and Monte Carlo simulation [20].

- 301 LHC. ROOT maintains an object-oriented structure, meaning it is organized around the
 302 data rather than the functions and logic. Its features include visualization tools such as
 303 histogramming, and statistical tools. ROOT can be used in C++ and python languages.
 304 Several subpackages exist for analysis such as RDataFrame.

305 3.1.1 TTree Introduction

306 ROOT provides a data structure called the TTree to store large amounts of columnar
 307 data efficiently. Usually scientific data is stored in what we call row-oriented formats such
 308 as a spreadsheet or CSV table. This format is well organized if one wants to access a single
 309 event, but viewing a single column then becomes inefficient, especially with large datasets.
 310 A TTree is columnar based, meaning it consists of a list of independent columns, called

311 branches. Examples of branches can be event IDs or particle kinematics such as momentum
312 in the x,y,z coordinates. Branches can hold integers, strings and std::vector data types.
313 Buffers are automatically allocated behind each branch. Buffers are temporary storage areas
314 for the independent binary version of the object. This is done to efficiently handle the writing
315 and reading of the data to and from disk. Also, each branch has one or more baskets, which
316 manages the in-memory buffer. In other words, a basket holds the values of a branch for a
317 number of consecutive events. When a buffer is full, it is optionally compressed and then
318 the corresponding basket is written to disk, leading to the creation of a new basket to hold
319 the next entries. ROOT allows users to change buffersize parameters of the branch for
320 personalized optimization. Figure 3.2 shows a more detailed flowchart of the TTree data
321 structure.

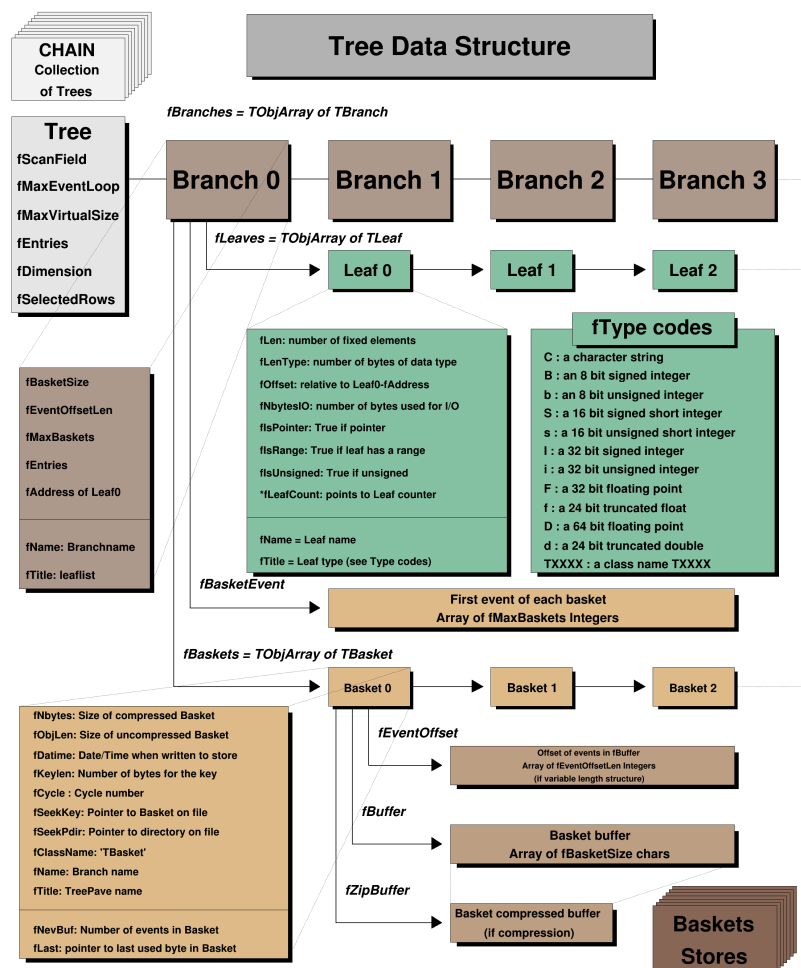


Figure 3.2: Example of the TTree Data Structure [21].

322

CHAPTER 4

323

RNTUPLE

324 RNTuple is the new columnar data format that will be implemented at the start of the
325 HL-LHC. It's design continues to be columnar based, as its predecessor TTree, but it now
326 uses modern storage technologies for better performance charactersitics in data compact-
327 ness, scalability and read and write speed. For this reason RNTuple classes are backwards-
328 incompatible to TTree both on the file format level and on the API level [23]. It's binary
329 format version follows an *epoch.major.minor.path* scheme, where *epoch* indicates backward-
330 incompatible changes, *major* indicates forward-incompatible changes, *minor* indicates new
331 optional format features, and *patch* indicates backported features from newer format veri-
332 ons. This chapter will introduce the RNTuple structure and user interfaces (UI) for different
333 workflows using the first public release of RNTuple 1.0.0.0.

334

4.1 Data Structure

335 RNTuple organizes data using an internal BLOB-based data layout and an external
336 metadata schema. A BLOB (binary large object) is a collection of binary data stored as
337 a single entity. For example, instead of embedding data directly into a database, data can
338 be stored as a BLOB along with a unique identifier for later retrieval. This is beneficial for
339 managing large unstructured data [25]. RNTuple uses a similar approach internally: Data is
340 organized by columns of a single type and are attached to *fields*, which describes a serialized
341 C++ type. Columns are partitioned into *pages*. Pages are compressed individually, similar
342 to TTree baskets. *Clusters* are sets of pages that contain all the data belonging to an entry

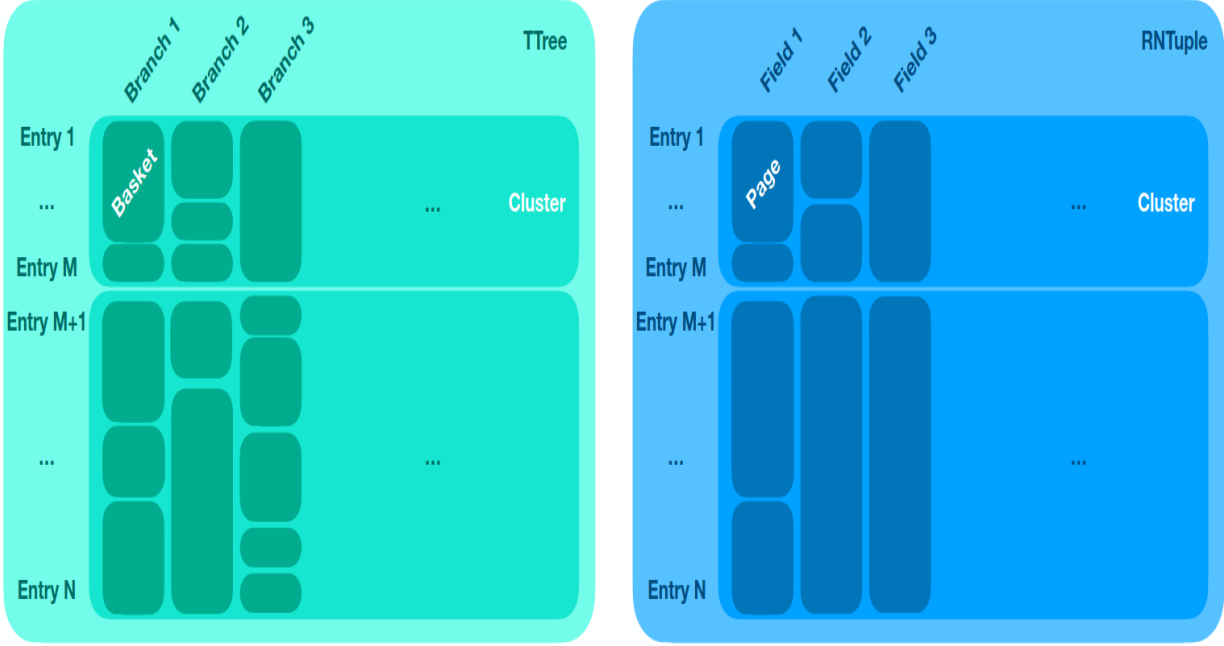


Figure 4.1: TTree Structure vs. RNTuple Structure [22].

³⁴³ range. *Envelopes* are data blocks that contain metadata, such as field and columns types,
³⁴⁴ cluster descriptions, and page locations. Overall, this structure allows for random-access
³⁴⁵ of individual events without decompressing the entire dataset and for "fast merging" or
³⁴⁶ concatenating RNTuples. A simplified diagram of the RNTuple structure in comparison to
³⁴⁷ TTree is shown in Figure 4.1.

³⁴⁸

4.2 UI

³⁴⁹ RNTuple API is compatible with RDataFrame analysis workflows and hand-written event
³⁵⁰ loops [24]. The sections below will provide further details and examples.

351

4.2.1 C++

352 For hand-written event loops, RNTuple interface uses smart pointers, which simulates
 353 a pointer while providing automatic memory management [26]. This feature shortens the
 354 amount of code necessary to read and load data by a couple of lines. For example `RNTupleReader::Open`
 355 simultaneously loads the ROOT file and the RNTuple. The function `GetView` also simulta-
 356 neously loads and stores a field. In the example below, the RNTuple is called "EventData"
 357 and the field is being stored into the object `electron_pt`, which is the transverse momentum
 358 of electrons, "AnalysisElectronsAux:pt".

```
359
360 1 auto ntuple = RNTupleReader::Open("EventData", "DAOD_PHYSLITE.pool.root");
361 2 auto electron_pt = ntuple->GetView<std::vector<float>>(
362     "AnalysisElectronsAux:pt");
363
```

364

4.2.2 RDataFrame

365 Analysis done with RDataFrame will mostly remain unmodified with RNTuple, with the
 366 exception of filtering. Due to RNTuple's internal data structure, subfields such as "Analysis-
 367 ElectronsAux:pt" are separated by their field, "AnalysisElectronsAux" by a column, instead
 368 of a period. This slight change confuses the filtering function in RDataFrame, but can be
 369 bypassed by assigning an alias name:

```
370
371 1 auto df = ROOT::RDF::RNTuple("EventData", "DAOD_PHYSLITE.pool.root");
372 2 auto new_df = df.Alias("electron_pt", "AnalysisElectronsAux:pt");
373 3 std::string analysis_cut = "(electron_pt.size() >= 1 & & electron_pt.at(0)
374     > 25000";
375 4 auto filtered_df = new_df.Filter(analysis_cut);
376
```

CHAPTER 5

RNTUPLE VS. TTREE

379 In this section, RNTuple performance is analyzed using RDataFrame in C++ and com-
 380 pared to TTree. First, 92 TTrees stored in DAOD_PHYSLITE files from ATLAS Open Data
 381 [30] were converted to RNTuples using its default compression algorithm setting, ZSTD.
 382 Speed tests were performed for loading and outputting RNTuples in comparison to TTrees
 383 using `std::chrono::high_resolution_clock::now()`. Each performance study contains
 384 two version: a TTree version that uses TTree inputs and an RNTuple version that uses
 385 the RNTuple inputs. A comparison of peak memory consumption was also performed using
 386 both sets of inputs. This entire process was repeated for RNTuple inputs converted with
 387 LZ4 compression algorithm as well.

5.1 Readability Speed

389 The total loading times for 92 RNTuples and their TTree equivalence were measured 100
 390 times. Loading multiple RNTuples in RDataFrame is the same procedure as done for the
 391 TTree version:

```
392
393 1 std::string path = "path_to_files";
394 2 std::vector<std::string> filenames;
395 3 for (const auto& entry: std::filesystem::directory_iterator(path)){
396 4     std::string filename = entry.path().filename().string();
397 5     filenames.push_back(entry.path().string());
398 6 }
399 7 auto df = ROOT::RDF::FromRNTuple("EventData", filenames);
```

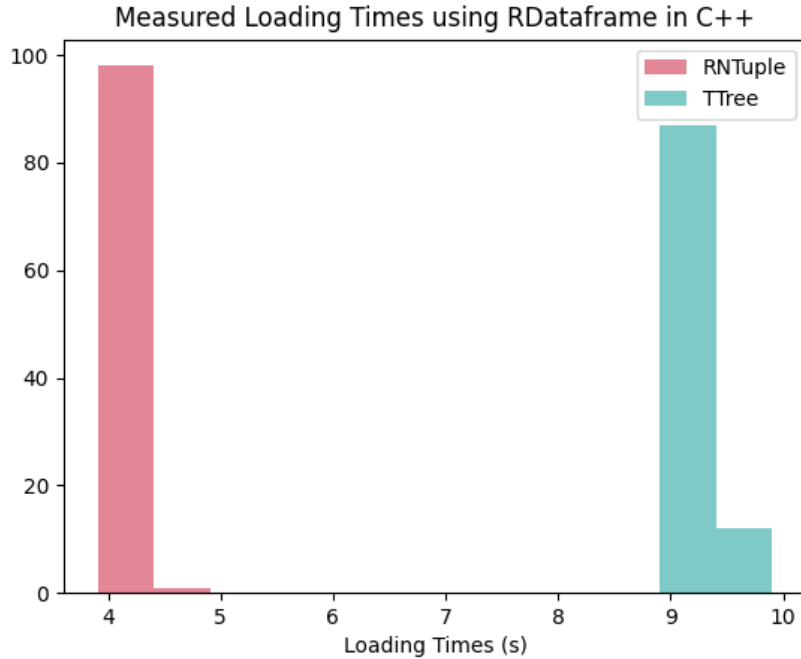


Figure 5.1: Total loading times measured for TTree and RNTuple using RDataFrame in C++.

The timer was stopped after calculating the sum of the column "AnalysisElectrons:pt" to ensure that the data was loaded. These times were recorded into a text file and are shown in Figure 5.1. In comparison, this study finds RNTuple to be 2.38 times faster at loading a column of data over TTree.

5.2 Writing Speed

406 Writing speed was measured by performing an invariant mass calculation and outputting
407 a new data set with two columns: "ElectronPairsInvMass" and "Muon PairsInvMass".
408 The timer began at the start of an invariant mass calculation and stopped after creating a
409 new dataset. A TTree was written for the TTree version and an RNTuple was written for
410 the RNTuple version. At the start of this study, the lazy function that outputs a TTree in

411 RDataFrame, df.Snapshot(...) was not developed to output an RNTuple; therefore, for
 412 consistency, both versions of the script used the RDataFrame function df.ForEach(...) to
 413 fill in the new columns. This procedure for RNTuple is shown below:

```
414
415 1 auto model = RNTupleModel::Create();
416 2 auto e_invm = model->MakeField<ROOT::VecOps::RVec<float>>("ElectronPairsInvMass");
417
418 3 auto m_invm = model->MakeField<ROOT::VecOps::RVec<float>>("MuonPairsInvMass");
419
420 4 auto ntuple = RNTupleWriter::Recreate(std::move(model), "Fat is RNTuple", "rnt_invm.root");
421
422 5 df_leptons.ForEach([&](ROOT::VecOps::RVec<float> e_vals, ROOT::VecOps::RVec<
423   float> m_vals){
424 6   *e_invm = e_vals;
425 7   *m_invm = m_vals; ntuple->Fill();
426 }, {"invm_electrons", "invm_muons"});
```

428 The total output times were recorded in a text file and are shown in Figure 5.2. RNTuple
 429 is shown to be 1.51 times faster at writing datasets in RDataFrame C++ than when using
 430 TTrees.

431 5.2.1 Output Sizes

432 After checking the disk sizes of the RNTuple outputs produced and comparing them to
 433 their TTree counterparts, RNTuple

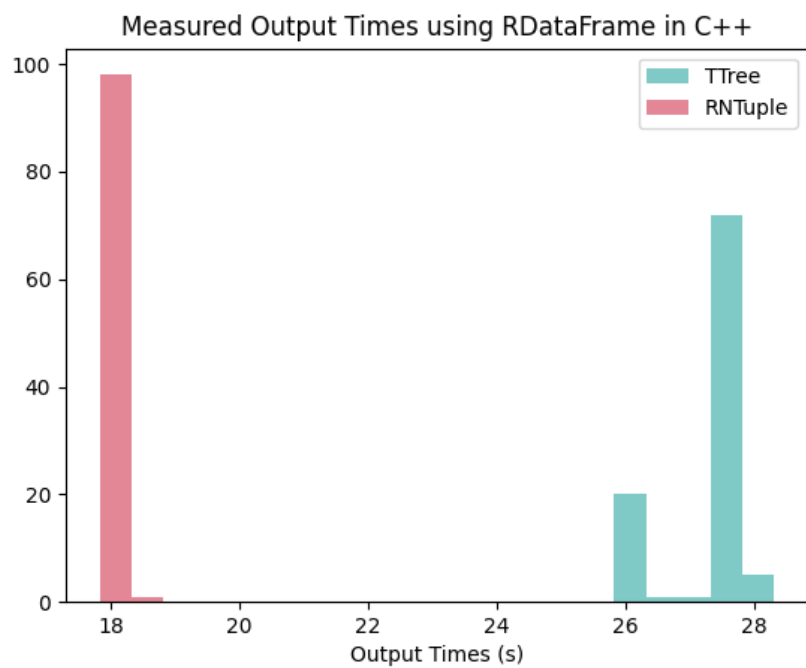


Figure 5.2: Total writing times measured for TTree and RNTuple using RDataFrame in C++.

, measurmeents taken show that RNTuple varies slightly from TTree.

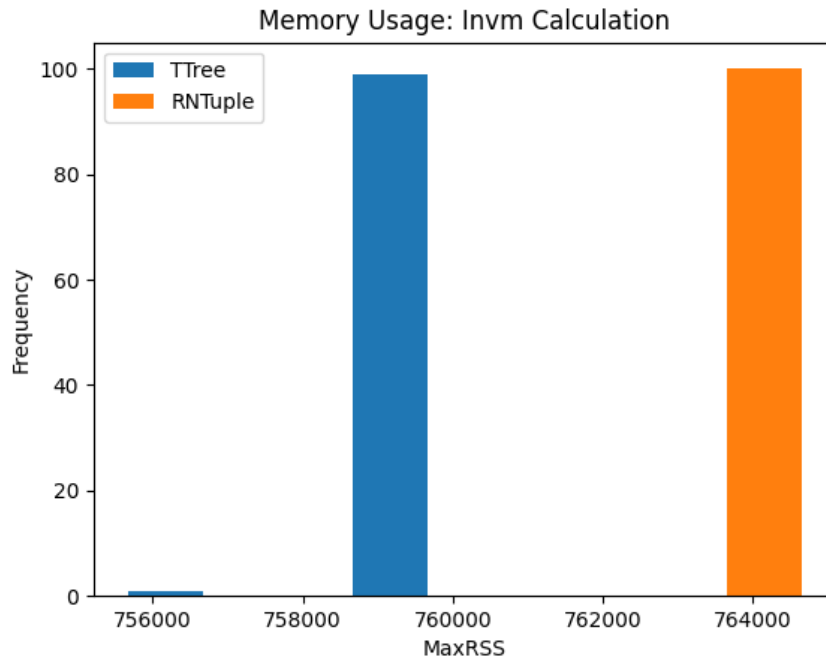


Figure 5.3: Peak memory measurments of TTree and RNTuple writing scripts [NOTE FOR FATIMA: CONSISTENT HISTOGRAM SHADING].

434

5.3 Memory Consumption

435

The peak memory usage when writing out a dataset was also measured for RNTuple and

436

TTree versions. The same procedure using the invariant mass calculation was repeated 100

437

times, but using the command `usr/bin/time`. Shown in Figure 5.3,

438

5.4 Compression Algorithms Study

439

[Under Construction]

440

CHAPTER 6

441

ANALYSIS GRAND CHALLENGE: RNTUPLE IMPLEMENTATION

442 The Analysis Grand Challenge (AGC) is an analysis on t quark production meant to
443 showcase an end-to-end analysis pipeline [49]. Developed and organized by Iris-HEP [48],
444 the AGC has several versions that showcase different cyber infrastructure and workflows,
445 making it a great benchmark to test RNTuple. This section will describe the development of
446 two new AGC versions that use ATLAS Open Data and RDataFrame: TTree and RNTuple
447 versions. These versions were heavily influenced on the existing RDataFrame AGC repository
448 that applies CMS open data and the uproot AGC repository that applies ATLAS open data
449 [49].

450

6.1 RDataFrame Analysis Workflow

451

The AGC is divided into two parts: an analysis script and a statistical script. The analysis scripts are written in Python and uses RDataFrame to apply preselections and output histograms of the top quark mass and the scalar sum of the transverse momenta, H_T , into a root file. The statistical script performs a simple statistical analysis using the output root file from the analysis script.

456

6.1.1 Event Selections

457

To reconstruct the top quark mass, events are selected from top quark pair production with final states that include a single charged lepton, as shown in Figure 6.1. The leptons

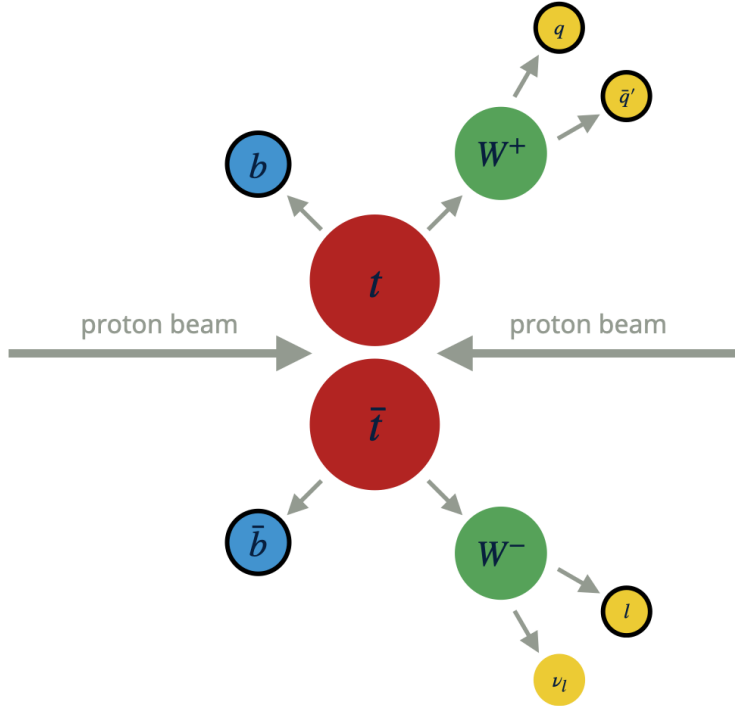


Figure 6.1: The schematic view of a top and anti-top quark collision [50]

must have p_t larger than 30 GeV and $|\eta|$ less than 2.1. Events must include four jets, with two of the four being "b-tagged". Jets that are "b-tagged" are matched to b and \bar{b} . The other two jets are from the W boson decay. The top mass observable is then reconstructed by taking the invariant mass of the trijet with the largest transverse momentum, p_t . The results are shown in Figure 6.2.

To plot the H_T observable, the selected events must have at least one b-tagged jet among the four jets and exactly one lepton. The results are shown in Figure 6.3.

6.2 TTree vs. RNTuple AGC

Both TTree and RNTuple versions of the AGC produced the outputs, confirming that analysis done in RDataFrame with RNTuple will mostly remain unmodified. As previously

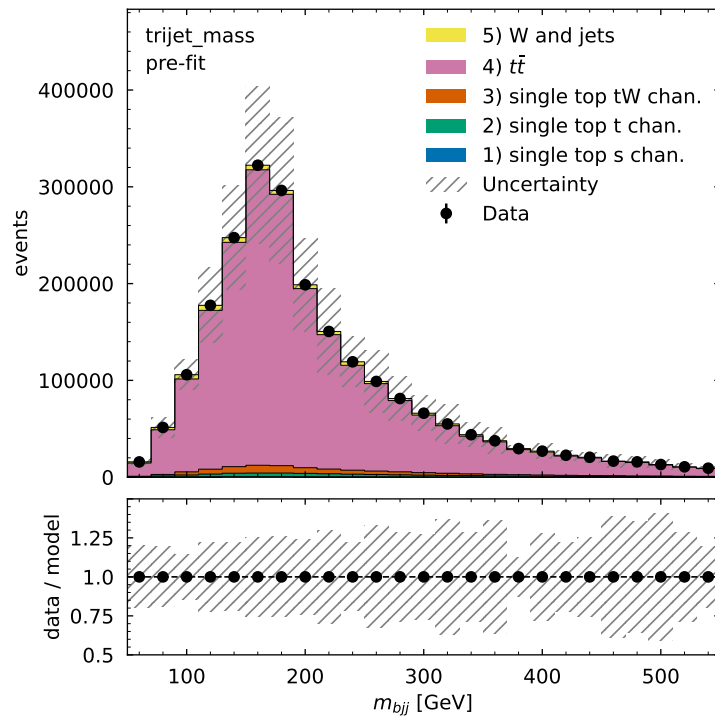


Figure 6.2: The trijet mass prefit. This result is the same for both RNTuple and TTree versions of the AGC.

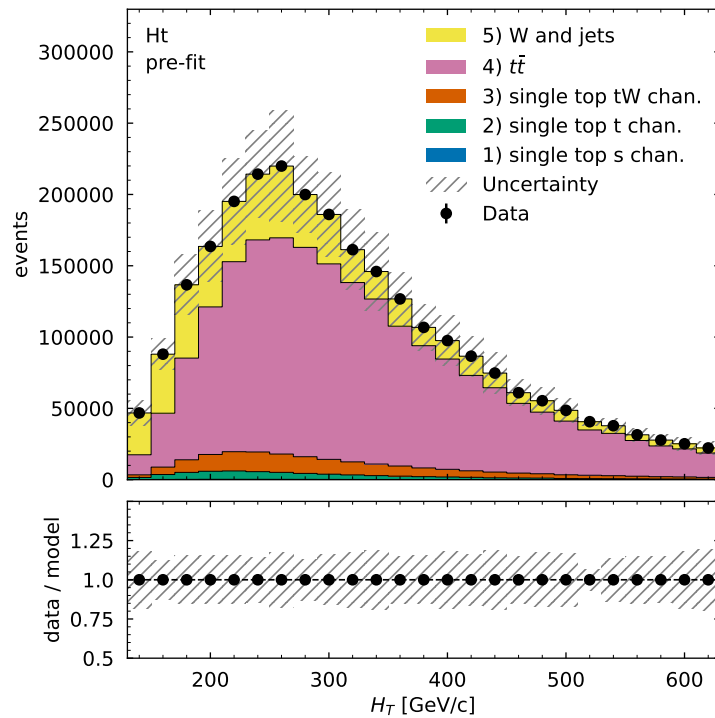


Figure 6.3: The H_T observable pre-fit. This result is the same for both RNTuple and TTree versions of the AGC.

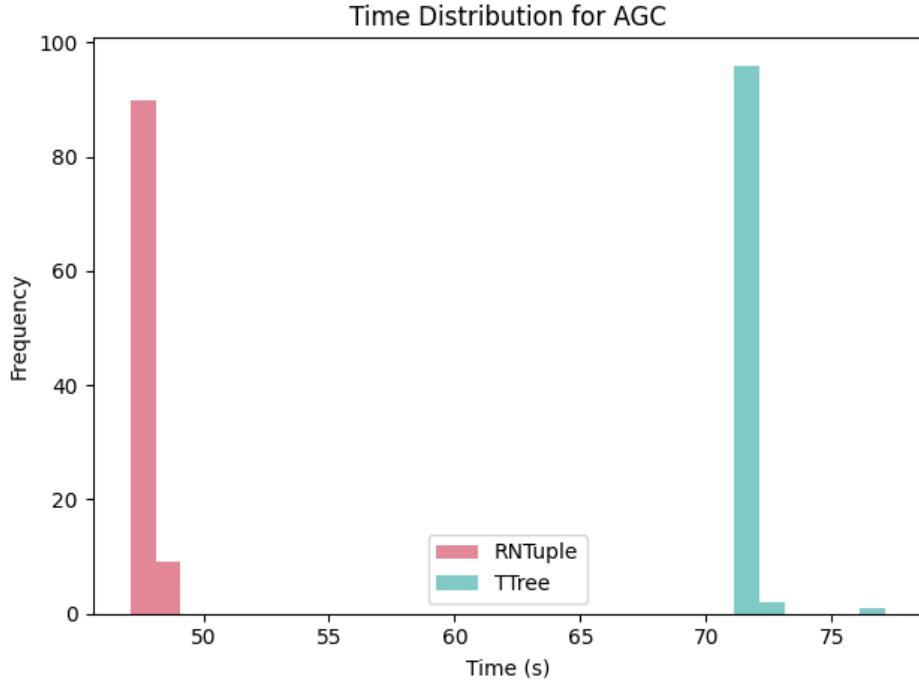


Figure 6.4: The total execution times of the AGC measured 100 times for TTree and RNTuple versions.

⁴⁶⁹ mentioned, RNTuple changes the structure of variable field names. For consistency, alias
⁴⁷⁰ variable names were applied to both TTree and RNTuple versions.

⁴⁷¹ 6.2.1 Timing Measurements

⁴⁷² Total execution times were measured 100 times for both TTree and RNTuple versions
⁴⁷³ using the time python library. Both versions used inputs produced with ZSTD compression
⁴⁷⁴ algorithm. The results, shown in Figure 6.5, show that RNTuple averaged 47.58 seconds
⁴⁷⁵ to produce the top quark mass and H_T histograms into a root file, while TTree averaged
⁴⁷⁶ 71.75 seconds. RNTuple was about 1.51 times faster, which is consistent with previous time
⁴⁷⁷ measurements shown in Chapter ??

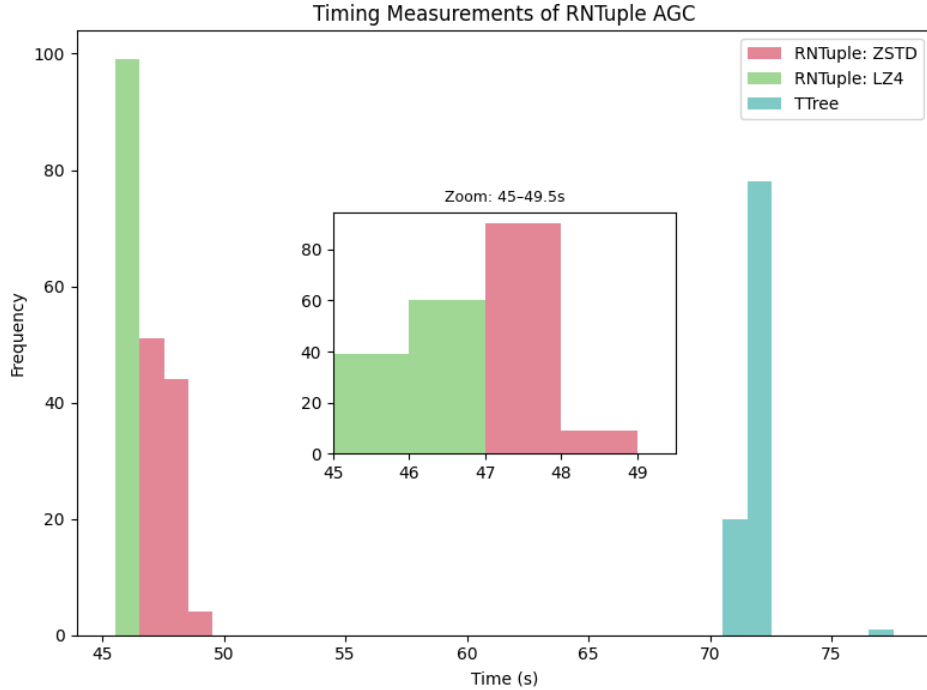


Figure 6.5: The total execution times of the AGC measured 100 times with RNTuples produced with LZ4 compression algorith.

478 6.2.1.1 LZ4 vs. ZSTD Input Files

479 The total execution times were remeasured using RNTuple inputs produced with the LZ4
 480 compression algorith. As shown in Figure ??, LZ4 executes the analysis script of the AGC
 481 about a couple seconds faster.

482 6.2.2 Memory Consumption

483 Peak memory usage was also measured using `/usr/bin/time`. The results shown in
 484 Figure ??, show that RNTuple consumes slightly less memory usage when executing the
 485 analysis script than TTree.

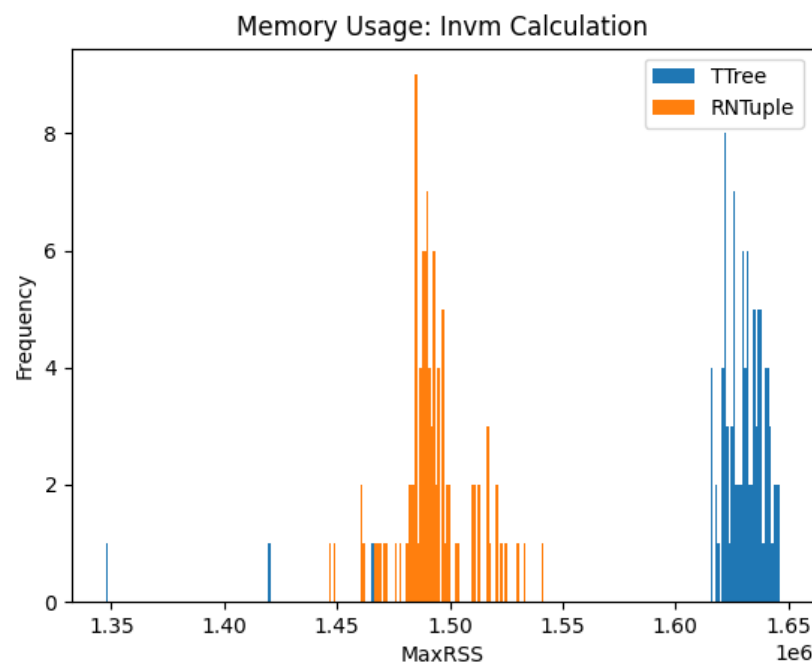


Figure 6.6: The peak memory usage when executing the AGC.

REFERENCES

- [1] ATLAS Collaboration. Standard Model summary plots. *ATLAS Public Note ATL-PHYS-PUB-2024-011*, 2024.
- [2] ATLAS Collaboration ATLAS: Letter of intent for a general purpose p p experiment at the large hadron collider at CERN. *CERN-LHCC-92-04*, 1992.
- [3] ATLAS Collaboration. The ATLAS experiment at the CERN Large Hadron Collider: a description of the detector configuration for Run 3. *JINST*, 19:P05063, 2024. URL: <http://dx.doi.org/10.1088/1748-0221/19/05/P05063>
- [4] R. Mann. *An Introduction to Particle Physics and the Standard Model*. Taylor & Francis, 2010. ISBN 978-1-4200-8300-2.
- [5] Wikipedia. Elementary particle. URL: https://en.wikipedia.org/wiki/Elementary_particle. Accessed: October 9, 2025.
- [6] C. N. Yang and R. L. Mills. Conservation of isotopic spin and isotopic gauge invariance. *Phys. Rev.*, 96:191–195, 1954.
- [7] P. W. Higgs. Broken symmetries, massless particles and gauge fields. *Phys. Lett.*, 12:132–133, 1964. DOI: 10.1016/0031-9163(64)91136-9.
- [8] P. W. Higgs. Broken symmetries and the masses of gauge bosons. *Phys. Rev. Lett.*, 13:508–509, 1964. DOI: 10.1103/PhysRevLett.13.508.
- [9] F. Englert and R. Brout. Broken symmetry and the mass of gauge vector mesons. *Phys. Rev. Lett.*, 13:321–323, 1964. DOI: 10.1103/PhysRevLett.13.321.

- 506 [10] G. S. Guralnik, C. R. Hagen, and T. W. B. Kibble. Global conservation laws and mass-
507 less particles. *Phys. Rev. Lett.*, 13:585–587, 1964. DOI: 10.1103/PhysRevLett.13.585.
- 508 [11] P. W. Higgs. Spontaneous symmetry breakdown without massless bosons. *Phys. Rev.*,
509 145:1156–1163, 1966. DOI: 10.1103/PhysRev.145.1156.
- 510 [12] ATLAS Collaboration. Observation of a new particle in the search for the Standard
511 Model Higgs boson with the ATLAS detector at the LHC. *Physics Letters B* 716.1
512 (2012), pp. 1-29
- 513 [13] CMS Collaboration Observation of a new boson at a mass of 125 GeV with the CMS
514 experiment at the LHC. *Physics Letters B* 716.1 (Sept. 2012), pp. 30-61
- 515 [14] L. Evans and P. Bryant. LHC machine. *JINST*, 3:S08001, 2008.
- 516 [15] E. Lopienska. The CERN accelerator complex layout in 2022. Complexe des acceler-
517 ateurs du CERN en janvier 2022. *CERN-GRAFICS-2022-001*, 2022. URL: <https://cds.cern.ch/record/2800984>
- 519 [16] J. Pequenao Computer generated image of the whole ATLAS detector. *CERN-GE-*
520 *0803012*, 2008. URL: <https://cds.cern.ch/record/1095924>
- 521 [17] J. Pequenao Computer generated image of the ATLAS inner detector. *CERN-GE-*
522 *0803014*, 2008. URL: <https://cds.cern.ch/record/1095926>
- 523 [18] J. Pequenao Computer generated image of the ATLAS Liquid Argon. *CERN-GE-*
524 *0803016*, 2008. URL: <https://cds.cern.ch/record/1095928>
- 525 [19] J. Pequenao Computer generated image of the ATLAS Muons subsystems. *CERN-GE-*
526 *0803017*, 2008. URL: <https://cds.cern.ch/record/1095929>

- 527 [20] J. Catmore The ATLAS data processing chain: from collision to paper. Joint
 528 Oslo/Bergen/NBI ATLAS Software Tutorial. University of Oslo, 2016. URL:
 529 https://indico.cern.ch/event/472469/contributions/1982677/attachments/1220934/1785823/intro_slides.pdf
- 531 [21] ROOT by CERN. TTree Class Reference. *ROOT Reference Guide*. URL: <https://root.cern.ch/doc/v630/classTTree.html>
- 533 [22] A. Serhan Mete,M. Nowak,P. van Gemmeren Persistifying the Complex Event Data
 534 Model of the ATLAS Experiment in RNTuple. *22nd International Workshop on Ad-*
 535 *vanced Computing and Analysis Technique in Physics Research*. 11-15 March 2024.
- 536 [23] ROOT Team Collaboration RNTuple Binary Format Specification 1.0.0.0 *CERN-*
 537 *OPEN-2025-001* (2024)
- 538 [24] J. Blomer,P. Canal,A. Naumann,D. Piparo Evolution of the ROOT TreeIO *EPJ Web*
 539 *of Conf.245* (2020) 02030
- 540 [25] Google Cloud What is binary large object (BLOB) storage? URL: <https://cloud.google.com/discover/what-is-binary-large-object-storage>
- 542 [26] Wikipedia Smart pointer URL: https://en.wikipedia.org/wiki/Smart_pointer
- 543 [27] ROOT Team ROOT Reference Documentation URL: <https://root.cern.ch/doc/master/index.html>
- 545 [28] J. Lopez-Gomez, J. Blomer RNTuple performance: Status and Outlook *J. Phys. Conf.*
 546 *Ser.2438* (2023) 1, 012118
- 547 [29] O. S. Bruning, P. Collier,P. Lebrun,S. Myers,R. Ostojic,J. Poole,P. Proudlock LHC
 548 Design Report *Geneva:CERN*,2024-548

- 549 [30] ATLAS Collaboration URL: <https://opendata.atlas.cern/>
- 550 [31] The ATLAS Collaboration. Athena *Zenodo*, (2019) DOI: <https://doi.org/10.5281/zenodo.2641996>
- 552 [32] J. Blomer,P. Canal,F. de Geus,J. Hahnfeld,A. Naumann,J. Lopez-Gomez,G. Lazari Miotto,V. E. Padulano ROOT's RNTuple IO Subsystem:The Path to Production
553
554 *EPJ Web of Conf.*295, 06020 (2024)
- 555 [33] Iris HEP Analysis Grand Challenge URL: <https://iris-hep.org/projects/agc.html>
- 557 [34] ATLAS Collaboration. The ATLAS Experiment: Trigger and Data Acquisition URL:
558 <https://atlas.cern/Discover/Detector/Trigger-DAQ>
- 559 [35] I. Bejar Alonso et al. "High-Luminosity Large Hadron Collider (HL-LHC): Technical
560 design report." *CERN Yellow Reports* Vol. 10 (2020)
- 561 [36] ATLAS Collaboration "Mass/Invariant mass" URL: <https://atlas.cern/glossary/mass>
- 563 [37] ATLAS Collaboration Facts Sheets "4-Vectors and particle mass" URL:
564 <https://cds.cern.ch/record/2919871/files/4-vectors%20and%20invariant%20mass%20cheat%20sheet.pdf>
- 566 [38] The ATLAS and CMS Collaborations. Highlights of the HL-LHC physics projections
567 by ATLAS and CMS. *CMS-HIG-25-002* 2025
- 568 [39] ATLAS Collaboration Technical Design Report for the ATLAS Inner Tracker Pixel
569 Detector, *CERN-LHCC-2017-021*, 2017.

- 570 [40] ATLAS Collaboration Technical Design Report: A High-Granularity Timing Detector
571 for the ATLAS Phase-II Upgrade. *CERN-LHCC-2020-007*, 2020
- 572 [41] ATLAS Collaboration Technical Design Report for the Phase-II Upgrade of the ATLAS
573 Muon Spectrometer. *CERN-LHCC-2017-017*, 2017.
- 574 [42] ATLAS Collaboration. ATLAS Liquid Argon Calorimeter Phase-II Upgrade : Technical
575 Design Report. *CERN-LHCC-2017-018*, 2017
- 576 [43] ATLAS Collaboration. Technical Design Report for the Phase-II Upgrade of the ATLAS
577 Tile Calorimeter. *CERN-LHCC-2017-019*, 2017.
- 578 [44] ATLAS Collaboration. Technical Design Report for the Phase-II Upgrade of the ATLAS
579 Tile Calorimeter. *CERN-LHCC-2017-019*, 2017.
- 580 [45] ATLAS Collaboration Technical Design Report for the Phase-II Upgrade of the ATLAS
581 TDAQ System. *CERN-LHCC-2017-020*, 2017
- 582 [46] S. Amato et al. LHCb technical proposal *CERN-LHCC-98-04*
- 583 [47] ALICE Collaboration ALICE: Technical proposal for a Large Ion collider Experiment
584 at the CERN LHC *Geneva: CERN*, 1995 - 237
- 585 [48] URL: <https://iris-hep.org/>
- 586 [49] URL: <https://iris-hep.org/projects/agc.html>
- 587 [50] URL: <https://github.com/alexander-held/PyHEP-2022-AGC/blob/main/talk.ipynb>

589

APPENDIX

590

OBJECTIVE SYMPTOMS

591 Appendices follow the same page-numbering rules as regular chapters. The first page of a
592 multi-page appendix is not numbered. But the page of a single-page appendix *is* numbered.

593 **Are they slow learners or is it a *REAL* problem?** These are classic findings in the
594 hopelessly computer challenged.

595 1. Can't copy from hard drive to disk.

596 2. Can't eject disks.

597 3. The word "disk" has thousands of meanings to them. None are correct.

598 4. Saving a document in any form is a concept totally unexplainable to them.

599 5. Desktop covered with Untitled Folders - look again, untitled folders are everywhere.

600 6. "Lost" documents found often in the Apple Menu.

601 7. Trash always full. Claim they don't know how to place things in trash.

602 8. Mysterious things happen to their documents or computer when they are not present.

603 AKA "computer victims".

604 9. Highlighting = deleting. Dragging = Oblivion.

605 10. Selecting, double-clicking a problem? They will always say their mouse is broken.

606 11. Their double- click mechanics wants you to send them to a neurologist.

607 12. Computer always on due to fear of having to restart it.

608 13. Have never read their QuickMail - will say "I prefer a phone call".

609 14. Have magical beliefs about what computers do.

610 15. Describes some flaky way computers could REALLY help them, but is not yet available.

- 611 16. Constantly saying they need more “memory”.
- 612 17. Requests gizmos and gadgets, i.e., “mouse leash” or “disk cozy”.
- 613 18. Avoids eye contact when talking about computers.